Geosci. Model Dev. Discuss., 7, 8975–9015, 2014
www.geosci-model-dev-discuss.net/7/8975/2014/
doi:10.5194/gmdd-7-8975-2014

Geoscientific Model Development Discussions
Open Access

Northern Hemisphere storminess in the Norwegian Earth System Model (NorESM1-M)

E. M. Knudsen[1,2] **and J. E. Walsh**[3]

[1]Geophysical Institute, University of Bergen, P.O. Box 7803, 5020 Bergen, Norway
[2]Bjerknes Centre for Climate Research, Bergen, Norway
[3]International Arctic Research Center, University of Alaska Fairbanks, 930 Koyukuk Drive, Fairbanks, Alaska 99775–7340, USA

Received: 17 November 2014 – Accepted: 26 November 2014
– Published: 16 December 2014

Correspondence to: E. M. Knudsen (erlend.knudsen@gfi.uib.no)

Published by Copernicus Publications on behalf of the European Geosciences Union.

Abstract

Metrics of storm activity in Northern Hemisphere high- and midlatitudes are evaluated from historical output and future projections by the Norwegian Earth System Model (NorESM1-M) coupled global climate model. The European Re-Analysis Interim (ERA-Interim) and the Community Climate System Model (CCSM4), a global climate model of the same vintage as NorESM1-M, provide benchmarks for comparison. The focus is on the autumn and early winter (September through December), the period when the ongoing and projected Arctic sea ice retreat is greatest. Storm tracks derived from a vorticity-based algorithm for storm identification are reproduced well by NorESM1-M, although the tracks are somewhat better resolved in the higher-resolution ERA-Interim and CCSM4. The tracks are projected to shift polewards in the future as climate changes under the Representative Concentration Pathway (RCP) forcing scenarios. Cyclones are projected to become generally more intense in the high-latitudes, especially over the Alaskan region, although in some other areas the intensity is projected to decrease. While projected changes in track density are less coherent, there is a general tendency towards less frequent storms in midlatitudes and more frequent storms in high-latitudes, especially the Baffin Bay/Davis Strait region. Autumn precipitation is projected to increase significantly across the entire high-latitudes. Together with the projected increases in storm intensity and sea level and the loss of sea ice, this increase in precipitation implies a greater vulnerability to coastal flooding and erosion, especially in the Alaskan region. The projected changes in storm intensity and precipitation (as well as sea ice and sea level pressure) scale generally linearly with the RCP value of the forcing and with time through the 21st century.

1 Introduction

The climate of the recent decades has undergone a warming that has been amplified in the Arctic. This polar amplification, due in part to the reduction of sea ice and

GMDD
7, 8975–9015, 2014

snow cover, has resulted in an Arctic warming that is twice as large as the global mean (e.g., Bekryaev et al., 2010; AMAP, 2011). The warming of the Arctic has contributed to, and been increased by, the loss of sea ice (Stocker et al., 2013). Other important factors contributing to polar amplification appear to be the lapse rate feedback, the increase in atmospheric humidity and the fact that longwave radiation to space increases less under global warming in the cold polar regions than in the tropics (the so-called Planck Effect) (Pithan and Mauritsen, 2014). Impacts of sea ice loss and Arctic warming on the atmospheric circulation in the high- and midlatitudes have been suggested by the studies of Overland and Wang (2010), Francis and Vavrus (2012) and Cohen et al. (2012), although the robustness of the midlatitude impacts has been questioned (Barnes, 2013; Barnes et al., 2014; Screen and Simmonds, 2013). Whether or not a large-scale signal of Arctic warming and sea ice loss has yet emerged from the noise of internal variability, climate models project continued Arctic warming and sea ice loss through the 21st century, increasing the likelihood of associated changes in the large-scale circulation.

Much of the effort to diagnose and project Arctic change has focused on temperature, sea ice and precipitation. However, climate-driven changes in storms are arguably more important considerations for Arctic residents, as well as for the heat and moisture budgets of the atmosphere. The impacts of storms are magnified by the loss of sea ice, which increases wave activity, coastal flooding and erosion and also increases the risks of vessel icing in waters newly accessible for marine transport and for other offshore activities.

The impacts of a warming climate on high-latitude storms are difficult to anticipate. On the one hand, the increased surface fluxes of heat and moisture might be expected to fuel more and stronger storms. On the other hand, polar amplification reduces the meridional baroclinicity upon which extratropical cyclones feed. While the net effect of these changing drivers is unclear, it is possible to assess changes in Arctic storminess from recent historical data and from global climate models run with prescribed external (greenhouse gas and aerosols) forcing.

GMDD
7, 8975–9015, 2014

Analyses of observational data have produced mixed results on trends of high-latitude storminess. In earlier studies, Zhang et al. (2004) found an increase of Arctic cyclone activity, while McCabe et al. (2001) reported northward shifts of storm tracks over the Northern Hemisphere (NH) over the last several decades of the 20th century. Wang et al. (2006) detected a northward shift of cyclone activity, primarily during winter, over Canada during 1953–2002, and this meridional shift was confirmed more generally in a more recent study by the same group (Wang et al., 2013). The recent US National Climate Assessment (Melillo et al., 2014) points to a poleward shift of storm tracks over the United States during recent decades. However, Mesquita et al. (2010) found that temporal trends of cyclones in the North Pacific Ocean have generally been weak over the 60 year period ending 2008. The U.S. Global Change Research Program (Karl et al., 2009) points to an increase of storminess on the northern Alaskan coast and to associated risks of flooding and coastal erosion. Since any increases of coastal flooding and erosion are also related to retreating sea ice, the role of storminess per se in increasing risk can be difficult to unravel.

Global climate models are arguably the best tools for identifying externally-forced signals in storm activity. In this study, we seek to validate the storm track components of two state-of-the-art global climate models over midlatitudes and high-latitudes of the NH. This is done through a comparison to a reanalysis data set. The models are the Norwegian Earth System Model version 1 with intermediate resolution (NorESM1-M) and the Community Climate System Model version 4 (CCSM4). The simulations examined here were performed as part of the Coupled Model Intercomparison Project phase 5 (CMIP5). After assessing the models' ability to capture the primary cyclone characteristics over a recent historical period, we compare the future changes of midlatitude and high-latitude storms through the late 21st century. The primary metrics of storm activity will be frequency (track density) and intensity. Since both models undergo further polar-amplified warming and the loss of much of their sea ice cover by the end of the century, the impacts of Arctic warming and sea ice loss on storm activity are implicit in our results.

GMDD
7, 8975–9015, 2014

The paper is organized as follows: Sect. 2 describes the models, reanalysis and methods used in this study. Section 3 presents the results of the comparison with the historical reanalysis and an overview of the primary changes in the storm metrics over the 21st century, followed by a discussion of the changes in the context of earlier studies and possible future implications. Finally, Sect. 4 concludes with a summary of the results, uncertainties and ideas for future work.

2 Data sets and methods

The present study uses two global climate models, NorESM1-M and CCSM4, both of which are coupled atmosphere–ocean–land–sea ice models. In keeping with the theme of this special issue, we emphasize NorESM1-M and its simulations. The output of CCSM4, which has somewhat finer resolution, is also examined since its storm simulations can serve as a benchmark for NorESM1-M. CCSM4 is described by Gent et al. (2011). The following is a more complete description of NorESM1-M.

NorESM1-M is a global, coupled model system for the physical climate system. It is a joint model effort of eight Norwegian research institutions, building on and replacing the Bergen Climate Model (BCM; Furevik et al., 2003) as the Norwegian CMIP model in the Intergovernmental Panel on Climate Change (IPCC) assessment reports.

NorESM1-M is described in more detail in Bentsen et al. (2013) and Iversen et al. (2013). It is based on CCSM4 and the Community Earth System Model (CESM) projects at the National Center for Atmospheric Research (NCAR) on behalf of the University Corporation for Atmospheric Research (UCAR) (Gent et al., 2011). However, NorESM1-M differs from CCSM4 in the following components: its own developed code for chemistry-aerosol-cloud-radiation interactions in the atmospheric module (CAM4-Oslo; Kirkevåg et al., 2013); an isopycnic coordinate ocean general circulation model developed in Bergen (e.g., Drange et al., 2005) and originating from the Miami Isopycnic Coordinate Ocean Model (MICOM; Bleck et al., 1992); and a biogeochemical ocean module from the HAMburg Ocean Carbon Cycle (HAMOCC) model developed at the

GMDD
7, 8975–9015, 2014

Max Planck Institute for Meteorology (MPI) in Hamburg (Maier-Reimer, 1993; Maier-Reimer et al., 2005) and adapted to the isopycnic ocean model framework (Tjiputra et al., 2010).

In this study, the first version of NorESM with intermediate resolution is presented. Known formally as NorESM1-M, the model has a horizontal resolution of approximately 2° for atmosphere and land components and 1° for ocean and ice components. Its vertical resolution consists of 26 levels of hybrid sigma-pressure coordinates with a model top of 2.9 hPa. For brevity, the model is denoted as NorESM throughout this paper.

CCSM4 has twice the horizontal resolution of NorESM, with 1.25° × 0.9° horizontal resolution and 26 vertical layers. de Boer et al. (2012) and other accompanying papers in the same CCSM4 special issue of the Journal of Climate assess the performance of CCSM4. For the remainder of this paper, CCSM4 will be denoted as CCSM for brevity. Apart from differences in the realizations, divergence between the two models highlight the role of the ocean, sea ice and atmospheric chemistry in the climate system with other model components being similar.

Only one ensemble member of each model (NorESM: r1i1p1, CCSM: r6i1p1) is examined in the present study because only these ensemble members meet our required criteria for temporal resolution (6 hourly output is needed for cyclone tracking) and choice of scenarios. However, Walsh et al. (2008) found that the spread within ensemble members of a single model is much smaller than inter-model spread when Arctic-averaged temperatures are compared.

The analysis involves three time periods of 27 years each and two Representative Concentration Pathways (RCPs). For the historical time period, 1979–2005, NorESM and CCSM are compared to the European Re-Analysis Interim (ERA-Interim; here abbreviated ERA-I) data set (Dee et al., 2011). ERA-I is a high-resolution reanalysis set in space and time. In this study, a 0.50° × 0.50° grid is used for all fields, interpolated from the highest available spatial resolution of 0.75° × 0.75°. The ERA-I data set is well suited for the northern regions (Jakobson et al., 2012; Chung et al., 2013), especially for storm tracking (Hodges et al., 2011; Zappa et al., 2013).

GMDD
7, 8975–9015, 2014

The future time periods are 2037–2063 (mid-century) and 2074–2100 (end of the century). For these two periods, both RCP4.5 and RCP8.5 are analysed (van Vuuren et al., 2011). These represent pathways with stabilization without overshooting to 4.5 $W m^{-2}$ by 2100, and continuous increase to 8.5 $W m^{-2}$ by 2100, respectively.

While the storm track analysis is based on 6 hourly zonal (u) and meridional (v) wind data, sea ice concentration (SIC), sea level pressure (SLP) and total precipitation (hereafter referred to simply as precipitation) examined here are monthly averages. All parameters are analysed over the extended autumn season September through December (SOND), which is the season of greatest ice retreat as shown in Table 1. The seasonal cycle of climatological monthly sea ice extent (SIE) for the past several decades is well captured by the two models, although both models show somewhat greater SIEs than the observational data during the autumn and early winter months (Table 1 and Langehaug et al., 2013, albeit reference for NorESM only). CCSM simulates slightly more rapid ice retreat then NorESM, although both models show the Arctic Ocean becoming ice-free (SIE < 1 million km^2) during the second half of the 21st century. The projected reduction of ice extent is greatest in the autumn and early winter, especially in terms of the percentage reduction from the historical values. Even the areal reductions are largest during this portion of the year. Moreover, the observed ice loss during recent decades (1979–present) is also greatest during the autumn (Stroeve et al., 2012; Rogers et al., 2013). In view of this seasonality, we focus our analysis on the SOND season.

The storm track analysis is based on the TRACK algorithm described by Hodges (1994, 1995, 1999). It uses 6 hourly 850 hPa relative vorticity (ζ) to identify and track cyclones, here calculated from the u and v fields. Rather than SLP, ζ is used for tracking due to the large independence from extrapolation, smaller influence of the large-scale background pressure field, and focus on the small-scale end of the synoptic range. This leaves many more systems identified. Moreover, ζ is more focused on the wind field while SLP is linked to the mass field, representing the low-frequency scale better (Hodges et al., 2003). Overall, Neu et al. (2013) found the number of storms identi-

GMDD
7, 8975–9015, 2014

fied by methods based on vorticity to be in the middle range of those obtained using different tracking algorithms.

The ζ field at moderate to high resolution can nevertheless be very noisy. Hence, to allow the same spatial synoptic scales to be identified in the three data sets, the analysis is performed at a spectral resolution of T42 on a Gaussian grid. Additionally, planetary scales with wave numbers below 5 and above 42 are removed to focus on the synoptic variability. Finally, criteria regarding their displacement distance (minimum 1000 km) and lifetime (minimum 2 days) are set. Only cyclones (not anticyclones) are considered.

For this study, two Eulerian statistical fields are of interest: the track density (a relative measure of how many cyclones pass through a region) and the mean intensity (a measure of the strength of the cyclones). These are computed by the spherical kernel estimators described in Hodges (1996). While the mean intensity unit corresponds to relative vorticity ($10^{-5}\,s^{-1}$), the track density is given in units of number density per month per unit area, where the unit area is equivalent to a 5° spherical cap ($\sim 10^6\,km^2$). Although changes of track density also could result from more (less) tightly confined cyclones, they are more likely due to an increase (decrease) in the number of cyclones. Hence, in the following, we refer to changes in the density fields as more or fewer cyclones.

Significance testing of the SIC, SLP and precipitation fields follow the Student's two-sided t test with a 5 % significance criterion. For the storm track characteristics, p values (the probability that a more extreme value is possible by chance) are computed using a permutation Monte Carlo approach (sampling without replacement) (Hodges, 2008). Correspondingly, grid points with $p < 0.05$ are denoted as significant in storm track figures.

Reanalyses are clearly incapable of capturing mesoscale low pressure systems (including "polar lows"), which have typical scales of 200–300 km and lifetimes generally shorter than two days (Condron and Renfrew, 2013). In a comparison of cyclones tracked from the ERA-40 reanalysis and from high-resolution satellite data, Condron

GMDD
7, 8975–9015, 2014

et al. (2006) have shown that the failure to capture mesoscale cyclones is especially problematic in the subarctic North Atlantic. The polar low climatologies of Zahn and von Storch (2008) and Bracegirdle and Gray (2008) also show maxima in the subpolar North Atlantic. In the present study, our coarse-resolution models are compared with the coarse-resolution ERA-I reanalysis using the same tracking algorithm, so there is general consistency in the resolution and by implication in the under-capture of cyclones. Nevertheless, the estimates of cyclones reported here from all three sources (ERA-I, NorESM, CCSM) are almost certainly low relative to the actual numbers, and our findings pertain only to systems of synoptic scale and larger.

3 Results and discussion

In the following, parameters representing storminess are presented. While Sect. 3.1 compares the representations of NorESM and CCSM to ERA-I, Sect. 3.2 shows the expected changes of these parameters towards the end of the century, as projected by NorESM and CCSM. Only the 2074–2100 time period following the RCP8.5 scenario is presented. This derives from the near-linear scaling of changes in sea ice, SLP, storm frequency and frequency, and precipitation with strength of scenario (RCP4.5 and RCP8.5) and time (1979–2005 to 2037–2063 and 2074–2100) in our results. Hence, we consider the 2037–2063 time period to be an intermediate state between the historical and 2074–2100 periods, and the RCP4.5 scenario to be mid-way to the RCP8.5 scenario.

Table 2 presents the main results of this study. Circumglobal averages spanning large areas, the averages for mid- and high-latitudes might cancel out variations within each region. However, the maps presented in Sects. 3.1 and 3.2 will disclose these features. The values in Table 2 are discussed in more detail in each section.

GMDD
7, 8975–9015, 2014

3.1 Historical time period

3.1.1 Sea level pressure

SLP is a large-scale measure of storminess. Storm activity generally increases with decreasing SLP as cyclones lower the SLP of a region as they track through.

Under the assumption that ERA-I represents the actual conditions, NorESM and CCSM reproduce the main SLP pattern, but both also show distinct biases (Fig. 1b and c compared to Fig. 1a). In midlatitudes (here defined 40–65° N), differences are small, with most of the variations due to the representation of the Siberian High (Table 2), which is slightly strengthened and shifted equatorwards in the two models (Fig. 1). This bias is strongest in NorESM that represents the Siberian High with SLP up to 1031 hPa compared to the maximum of 1027 hPa in ERA-I.

Contrary to the southward-shifted Siberian High, the local minima of the Aleutian and Icelandic lows are shifted polewards in the two models (Fig. 1b and c compared to Fig. 1a). NorESM and CCSM have high-latitude (here defined 65–90° N) SLP biases of −2 and −6 hPa, respectively.

The substantial SLP bias in CCSM was also noted by DeWeaver and Bitz (2006), who compared the two resolutions T42 and T85 of CCSM3 (CCSM version 3) to the National Centers for Environmental Prediction (NCEP)/NCAR reanalysis. They found the bias to be more pronounced in the higher resolution, and ascribed this deficiency to the model's inability to simulate the Beaufort High in autumn, winter and spring. de Boer et al. (2012) showed that this same bias persists in CCSM4.

3.1.2 Track density

Figure 2 shows the distribution in cyclone frequency in the three data sets. The two main storm tracks of the North Atlantic and the North Pacific oceans are apparent, and likewise the local maxima over Canada and northern Eurasia.

GMDD
7, 8975–9015, 2014

Compared to ERA-I, both models depict poleward-shifted storm tracks over the North Pacific Ocean, Canadian Arctic and the Nordic Seas (Fig. 2b and c compared to Fig. 2a). On the contrary, the eastern branch of the North Atlantic storm track is broader and extends farther south in the models. These features offer an explanation for the poleward-shifted and wider low SLP bands in Fig. 1. For the North Atlantic Ocean overall, cyclones in NorESM and CCSM are slightly too zonal compared to ERA-I, consistent with the winter pattern found in CMIP5 models by Zappa et al. (2013). This leaves fewer cyclones tracking through the Greenland Sea – the region where most Arctic cyclones track (Sorteberg and Walsh, 2008).

In CCSM, the number of cyclones within the domain of 40–90° N is 7 % higher than in ERA-I, mainly due to the discrepancy in high-latitudes (Table 2). On the contrary, there are 2 % fewer cyclones in NorESM than found in ERA-I. For NorESM, this anomaly stems from its resolution, which is about four times as coarse as in the reanalysis. This leaves fewer cyclones resolved (Hodges et al., 2011).

The signal in CCSM offers an additional explanation to the large-scale background SLP bias discussed in Sect. 3.1.1: as more cyclones are resolved in CCSM compared to ERA-I (Table 2), a particular grid point in the main storm track will experience lower SLP for more time steps, understandably dependent on the cyclone strength. This is indicated by the anomalous low SLPs in the two main storm tracks in Fig. 1c compared to Fig. 1a. Why CCSM gives more cyclones than ERA-I in the first place is unknown, but might reside in its distribution of sea surface temperature or sea ice, or of different parameterization, e.g., for convection.

Moreover, most of the discrepancy relative to ERA-I stems from the high-latitudes south of the Arctic Ocean, with 14 % more cyclones in CCSM over the band 55–65° N. This could point to a closer similarity of CCSM to the Arctic System Reanalysis (ASR) over ERA-I, as found by Tilinina et al. (2014). They detected 30–40 % more cyclones over high-latitude continental areas in summer and winter in the ASR compared to ERA-I and other global modern era reanalyses, ascribing the anomaly mostly to moderately deep and shallow cyclones.

GMDD
7, 8975–9015, 2014

3.1.3 Mean intensity

The average strength of cyclones per unit area is presented in Fig. 3. Since regions of numerous cyclones are likely also to include more intense cyclones than other regions, the mean intensity pattern generally follows the track density pattern in Fig. 2. However, cyclones are stronger over ocean than land and vary with temperature through baroclinicity.

Corresponding to the contraction of the low SLP fields in the North Atlantic and the North Pacific oceans (Fig. 1), the mean intensity maxima are shifted polewards in the two models compared to ERA-I (Fig. 3b and c compared to 3a). Accordingly, the intensity minima are shifted equatorwards with the positive SLP bias over North America and Eurasia. The latter shift is to a lesser extent reproduced for track density (Fig. 2), indicating the stronger dependence of SLP on cyclone strength when compared to frequency (cf. SLP bias discussion in Sect. 3.1.2). Moreover, model biases in mean intensity generally follow those of SLP, where lower (higher) SLP corresponds to stronger (weaker) cyclones (Table 2).

In addition to the displacement of the density features in the two models compared to the reanalysis, cyclones are generally weaker in cyclone-dense regions and stronger in cyclone-light regions (Fig. 3). As with track density (Fig. 2), the values in NorESM are generally lower.

Our results add to the CMIP5 model underestimation of cyclone intensities in the North Atlantic Ocean in winter and summer compared to ERA-I found by Zappa et al. (2013). Specifically, Fig. 3 shows that cyclones are generally weaker in the two CMIP5 models NorESM and CCSM in the extended autumn season.

3.1.4 Precipitation

Precipitation is an indirect measure of storminess. Cyclone-dense regions are characterized by high frontal precipitation, with orographic precipitation reaching high levels when cyclones track into mountainous land.

GMDD
7, 8975–9015, 2014

Figure 4 shows the average pattern of precipitation for NH midlatitudes and high-latitudes over the historical time period. Some key features stand out. Firstly, frontal precipitation accounts for a large fraction of the precipitation, as seen from the close similarity between the precipitation (Fig. 4) and cyclone track density fields (Fig. 2).

Secondly, orographic precipitation is the second most important component to the precipitation. This can be seen from the maxima where the main storm tracks reach land (the west coasts of North America, Scotland and Norway, and the south coasts of Greenland and Iceland). Moreover, local maxima in connection with the Rocky and Cantabrian mountains, the French and Dinaric alps, as well as Caucasus and the mountains of Japan point to the role of the water bodies to the west of these mountains. As the westerly wind crosses these waters, the air gains moisture that later result in orographic precipitation on the windward side of the mountains as the air is forced upwards.

Frontal precipitation is represented reasonably well in NorESM and CCSM (Fig. 4b and c compared to Fig. 4a, and Fig. 4 compared to Fig. 2). However, in the North Atlantic Ocean, both models give the precipitation field an orientation that is too zonal in the western half and too meridional in the eastern half. As a consequence, considerably more precipitation falls in the northeastern corner of the North Atlantic Ocean.

The orographic precipitation maxima in the two models are shifted towards the east or northeast compared to ERA-I (Fig. 4b and c compared to Fig. 4a). This is likely a result of the resolution difference, in which elevation gradients are smoothed (i.e., weakened) over larger grid boxes. With a prevailing westerly wind in the domain, the air "feels" the mountains later (i.e., farther east) in NorESM and CCSM than in ERA-I. Moreover, the coarse resolution of NorESM restricts the ability to represent orographic precipitation, so the orographic maxima in NorESM are too weak (Fig. 4b).

For this reason, and due to the fewer cyclones resolved (Sect. 3.1.2), we would expect to see less precipitation in NorESM than ERA-I. However, the difference over the domain is only a 1 % reduction (Table 2). This might indicate that cyclone frequency has a greater impact on precipitation than cyclone strength, as the corresponding negative

GMDD
7, 8975–9015, 2014

biases over the domain for track density and mean intensity are 2 and 5 %, respectively. CCSM, with both more and stronger cyclones, has 10 % more precipitation over the domain than does ERA-I (Table 2).

3.2 Future scenario changes

In addition to the circumglobal averages over mid- and high-latitudes in Table 2, projected changes in storminess parameters (track density, mean intensity and precipitation) were evaluated for four chosen regions. The regionally averaged parameters are summarized in Table 3.

The regions, pictured in Fig. 6a, were chosen to enable the assessment of a potential shift in the two main historical storm tracks, the North Pacific and North Atlantic storm tracks. The western North America (WNA) and northwestern Europe (NWE) represent the landfall of the main storm tracks in the historical time period, while their northerly neighbouring regions Bering and western Alaska (BWA) and northeastern Europe (NEE) constitute the stormier regions that could result from poleward-shifted storm tracks (see Table 3 for latitudinal and longitudinal boundaries). The four regions have very similar areas and are thus intercomparable.

The numbers of each parameter and each model in Table 3 are discussed in Sects. 3.2.2, 3.2.3 and 3.2.4.

3.2.1 Sea level pressure

Compared to the 1979–2005 historical time period, both models show a significant reduction of 2 hPa in the SLP field over high-latitudes by the end of the century (2074–2100; Table 2 and Fig. 5). We attribute this, at least in part, to the sea ice retreat (Table 1). With a later refreezing, the autumn air temperatures – although warmer than today (Overland et al., 2013) – create a substantial temperature gradient with the warmer ocean temperature. The result is high heat fluxes from the ocean to the atmosphere,

GMDD
7, 8975–9015, 2014

destabilization of the air column and lowered SLP. Baroclinicity is also enhanced by the greater horizontal temperature contrast between land and open ocean during autumn.

Both models also indicate a significant increase in SLP over the North Atlantic Ocean, reaching 4 hPa west of the British Isles in NorESM (Fig. 5). Moreover, they both suggest increased pressures over eastern North Pacific Ocean, albeit CCSM insignificantly. However, due to the significant SLP reduction around the Sea of Okhotsk, the average midlatitude changes are negligible (Table 2).

The patterns in Fig. 5 bear resemblance to the positive phase of the Arctic Oscillation (AO). This is indicative of a poleward-shifted jet stream, which steers storms eastwards to the north of their usual paths and leaves midlatitudes with fewer cold air outbreaks than usual (Thompson and Wallace, 2001).

3.2.2 Track density

According to NorESM and CCSM, fewer cyclones will track along the current main storm tracks in the North Atlantic and North Pacific oceans towards the end of the century (Fig. 6). This explains the 3.9–6.5 % reductions in midlatitudes found in Table 2. On the other hand, there is a tendency of more cyclones tracking in parts of the Nordic and Bering seas (mostly in NorESM), indicating poleward-shifted storm tracks. This tendency has also been noted in previous studies (e.g., Wang et al., 2006, 2013; Sorteberg and Walsh, 2008). However, averaged over high-latitudes, the projected changes in cyclone frequency are negligible (Table 2), in contrast to the observed significant increase found by McCabe et al. (2001) over 60–90° N for November through March. Nevertheless, the observed enhancement of cyclones is found to be lower in autumn than in other months (Sepp and Jaagus, 2011).

Figure 6, as well as Figs. 7 and 8, show projected storminess parameters in the initial and final months September and December instead of the SOND average to highlight the transition over the season. This seasonality is more distinct for track density, mean intensity and precipitation than SLP.

GMDD
7, 8975–9015, 2014

NorESM shows a distinct seasonality in projected changes of cyclone frequency. While there is an indication of poleward shifts of the two main storm tracks in both September and December, these are more distinct in the first month (Fig. 6a and c). Moreover, significantly more cyclones track into the Arctic Ocean in September, with the opposite being the case for December. An antiphase between the two months is also apparent over large parts of Asia and North America (Fig. 6a and c).

The seasonal variation of projected changes in cyclone frequency is less distinct in CCSM (Fig. 6b and d). The September pattern for the Arctic Ocean differs from that of NorESM by a general decrease in number of cyclones (Fig. 6b compared to Fig. 6a). Even though the patterns are more similar in December, CCSM indicates significant increases of frequencies along the Siberian and west Alaskan coasts, where NorESM projects changes of opposite sign (Fig. 6d compared to Fig. 6c).

The variability in the North Pacific storm track severely determines the day-to-day weather conditions in the coastal regions of western Canada and southern Alaska. The same can be said of the North Sea region from the North Atlantic storm track, represented by the variably wet and windy climates of the British Isles and southern Scandinavia (Figs. 2, 3 and 4).

The poleward-shifted North Pacific storm track results in 8.0–20.1 % fewer cyclones reaching the North American west coast in the two models in September and in CCSM in December (Table 3 and Fig. 6a, b and d). Simultaneously, more cyclones track into Bering Sea, clearly indicating a poleward shift of the North Pacific storm track. In CCSM, increase of cyclones does not reach the Bering Strait in September, explaining the 8.1 % reduction in Table 3.

The NorESM December pattern (Fig. 6c) differs from the other three panels in Fig. 6, with opposite changes in the North Pacific sector of nearly equivalent size. The 18.2 % increase in WNA and 13.4 % decrease in BWA in September contrast with the corresponding decrease of 20.1 % and increase of 11.3 % in September. While both months show a poleward-shifted storm track, the December track is more zonal, giving more cyclones in a band over about 50–60° N from southeastern Russia to the Gulf of Alaska

GMDD
7, 8975–9015, 2014

(Fig. 6c). Fewer cyclones track over the Bering Strait and into the Arctic Ocean, possibly contributing to the marked difference between September and December here (Fig. 6a compared to Fig. 6c).

In the North Atlantic sector, NorESM has a more uniform projection in cyclone frequency over the two months (Fig. 6a and c). The poleward-shifted storm track leaves up to 12.8 % more cyclones reaching Scotland and southern Norway, but the reduction in the North Sea region in December contributes to a 5.9 % decrease overall in NWE (Table 3). This corresponds to the 8.9 % reduction in CCSM in December, with an even greater reduction of 21.7 % in September. In the latter month, remaining storms in CCSM seem to take more meridional paths, either over the Labrador Sea and Baffin Bay or over the Greenland Sea (Fig. 6b). The former regional change corresponds to the observed trend found by Sepp and Jaagus (2011).

3.2.3 Mean intensity

Towards the end of the century, cyclones generally weaken over midlatitudes (including the main storm tracks) and strengthen over high-latitudes (Table 2 and Fig. 7). This corresponds to the overall picture in Fig. 6, although the high-latitude amplification is clearer for intensities (Table 2). On the other hand, the weakening in midlatitudes is smaller, with an average 2 % reduction in mean intensity over the domain of the two models compared to 4 % decrease in track density. In other words, while there is a projected decrease in number of storms crossing the North Atlantic and the North Pacific oceans, their strength will not drop proportionally. We propose this feature is a result of the overall warming, where higher temperatures and corresponding increases of atmospheric moisture generally favour stronger cyclones. However, no systematic changes were detected in the lifetime of the systems over the century (not shown), in contrast to the positive trend detected in reanalysis data by Wang et al. (2013).

The results discussed here support the findings of McCabe et al. (2001). They found an insignificant increasing historical trend in winter storm intensity on top of a significant decrease in cyclone frequency over midlatitudes. Moreover, using BCM, Orsolini and

GMDD
7, 8975–9015, 2014

Sorteberg (2009) projected a 3.1–4.6 % drop in the total number of summer cyclones in the NH over the century, but also saw a slight storm intensification in high-latitudes.

For September, both NorESM and CCSM project a significant increase in cyclone strength over the Arctic Ocean (Fig. 7a and b). By the end of the century, the Arctic is essentially ice-free by September in NorESM and CCSM (Table 1 and green lines in Fig. 7a and b). Hence, as the atmosphere cools off more rapidly than the ocean, strong vertical gradients of temperature and moisture arise. Heat fluxes enter the atmosphere, destabilize the air column and thus foster the cyclones. Additionally, the enhanced latent heat release and reduced friction (and low-level convergence) due to the sea ice melt might also intensify the cyclones. This intensification might account in part for the SLP deepening over the Arctic seen in Table 2 and Fig. 5. Stronger cyclones have lower SLP, and this tendency is consistent with the observational results of Sepp and Jaagus (2011).

The heat flux potential is even stronger in December when the temperature gradient between the ocean and the atmosphere is greater. As a result, the now ice-free areas of the Sea of Okhotsk, Bering and Chukchi seas are projected to be characterized by more intense cyclones (Fig. 7c and d). However, only minor changes are found along the Atlantic sea ice edge, and NorESM also indicates a significant decrease in cyclone strength over most of the Arctic Ocean (Fig. 7c). The latter feature is most likely a result of the significant reduction of the number of cyclones (Fig. 6c), where the tendency for fewer cyclones is expected to degrade the likelihood of strong cyclones. Conversely, in the rapidly winter-warming Russian sector (Stocker et al., 2013), cyclones are projected to become more intense (Fig. 7c and d) and, in NorESM, also more numerous (Fig. 6c).

According to the two models, cyclones generally weaken in WNA (up to 6.2 %) and strengthen in BWA (up to 8.3 %) in September and December (Table 3 and Fig. 7). This mainly follows from the poleward-shifted storm track and track density pattern discussed in Sect. 3.2.2, although the negligible change in cyclone intensity starkly contrasts the 18.2 % increase in cyclone frequency in WNA for December in NorESM (Table 3) – especially if one would have expanded the region southward. In the coastal re-

GMDD
7, 8975–9015, 2014

gions from Oregon to British Columbia, the number of cyclones significantly increases while their strength significantly decreases (Fig. 6c compared to Fig. 7c). The opposite holds true in BWA (Table 3), demonstrating the closer resemblance between the two models for mean intensity than track density.

The projected changes in cyclone frequency and intensity along the North American west coast extend the results of Vose et al. (2014). Along this coast, they found a tendency of enhanced cyclonic activity (number and intensity) in the American sector and reduced activity in the Canadian sector over 1979–2010 compared to 1948–1978 during the cold season. These tendencies coincided with raised wave heights from the Baja California peninsula to the Aleutian Islands, emphasizing the importance of correct cyclone projections with regards to flooding, erosion and coastal activities.

In NWE, cyclones weaken by 5.9–8.9 % in September and intensify by 1.3–4.2 % in December (Table 3). This is indicative of a delayed seasonality, in which the autumn storms in this region come later in the year (not shown). The signal for NEE is less clear, although the changes for the continental areas of the region seem to be anticorrelated with the corresponding continental changes in NWE (Fig. 7).

Bengtsson et al. (2006, 2009) found that storms are likely to become less frequent and less intense at midlatitudes, but more numerous and stronger at high-latitudes by the late 21st century compared to the late 20th century. Although mainly focusing on the winter (DJF) and summer (JJA) seasons, the NH averaged signal was also apparent in the autumn (SON) season. Our results in Figs. 6 and 7 strengthen this conclusion, as we would also anticipate a further decrease equatorwards of 40° N.

3.2.4 Precipitation

Both models project significantly wetter conditions in high-latitudes by the end of the century compared to the historical time period, with the SOND mean rising 31.8–38.2 % (Table 2). As seen in Fig. 8, this applies to both September and December. However, differences between September and December are apparent in midlatitudes. While there is an overall increase also here (8.0–10.7 %; Table 2), large areas of reduced

GMDD
7, 8975–9015, 2014

precipitation occur in September (Fig. 8a and b). These are mainly the eastern North Pacific and North Atlantic oceans, the latter giving most of Europe drier conditions by the end of the century.

The projections give southern Europe less precipitation also for December, but the regions of enhanced precipitation are expanded over the rest of the domain at this time of year (Fig. 8c and d). Part of the reason is the poleward-shifted storm tracks, which are more significant for September than December (Sects. 3.2.2 and 3.2.3). This is indicative of the wet-get-wetter, dry-get-drier pattern reported elsewhere (e.g., Held and Soden, 2006; Stocker et al., 2013).

The largest increases in precipitation are found along the shifted main storm tracks and in regions of enhanced cyclone frequency and strength (Figs. 6 and 7), in accordance with the near doubling along the cyclone tracks relative to the global mean increase found by Bengtsson et al. (2009). At the landfall of the shifted storm tracks, western Alaska and northern Scandinavia are projected to see much stormier and wetter autumns by the end of the century.

In addition to the Mediterranean Sea, the eastern North Atlantic Ocean also becomes significantly drier in the projections (Fig. 8). The reason for this is not firmly established, although a poleward migration of the Hadley Cell's downward limb is thought to be part of the reason (Kang and Lu, 2012). This region is projected to warm less than the rest of the NH, with relatively lower humidity potential for increased atmospheric moisture (Stocker et al., 2013). Moreover, NorESM and CCSM show partly reductions in cyclone frequency and intensity in the eastern North Atlantic Ocean/Mediterranean region (Figs. 6 and 7).

The two models generally agree, but NorESM expands the wetter projection over a larger area of North America in December (Fig. 8c compared to Fig. 8d). In contrast, the pattern over Europe shows greater seasonal change in CCSM, with a wider region of less precipitation in September (Fig. 8b compared to Fig. 8a) and a wider region of more precipitation in December (Fig. 8d compared to Fig. 8c). Averaged over the 40–90° N domain for SOND, the two models both project 0.3 mm d^{-1} more precipitation.

GMDD
7, 8975–9015, 2014

This overall increase of precipitation is consistent with an increase of temperature and the ability of warm air to contain more moisture, resulting in an acceleration of the hydrologic cycle (Held and Soden, 2006).

Of the four regions, two months and two models in Table 3, only Septembers over the WNA region in NorESM and over the NWE region in CCSM are projected to become drier (4.1 and 12.0 %, respectively). However, compared to the significant increase in precipitation over the domain (Table 2 and Fig. 8a and b), the 5.8 and 5.7 % increases in WNA in CCSM and NWE in NorESM, respectively, are relatively small, too. Again, the poleward-shifted North Pacific and North Atlantic storm tracks are likely causes, leaving Septembers in the more northern BWA and NEE wetter by 11.7–23.8 % (Fig. 6a and b). More cyclones in the Bering, North and Greenland seas partly explain the significant increase in precipitation over the continental area to their east: Alaska, southern and northern Norway (Figs. 6a and b, 8a and b).

In December, the poleward storm track shift is less significant (Fig. 6c and d), giving 8.7–19.7 % more precipitation in WNA and NWE (Table 3 and Fig. 8c and d). The models still project significantly wetter conditions in BWA and NEE (although with an exception of NEE in CCSM; Fig. 8d), highlighting the increased availability of warmer air to hold moisture in the most rapidly warming region and season (Stocker et al., 2013).

Totalled over the full season SOND, the projected changes in precipitation in Fig. 8 might have severe consequences for multiple regions. Two of these are the Norwegian west coast (here defined 58–63° N, 5.0–7.5° E) and the Gulf of Alaska (here defined 58–63° N, 135–155° W). They are currently among the wettest regions in the extratropical NH. If we would believe the projections from the models, an additional 39 (CCSM) to 132 mm (NorESM) and 71 (NorESM) to 115 mm (CCSM) precipitation will fall over the Norwegian west coast and the Gulf of Alaska, respectively, over each SOND season during the years 2074–2100 compared to 1979–2005.

GMDD
7, 8975–9015, 2014

4 Conclusions

In this study, we have used a vorticity-based storm-tracking algorithm to analyse changes in metrics of storminess in mid- and high-latitudes through 2100 in the NorESM1-M global climate model. The main findings obtained from NorESM1-M are generally supported by the results obtained from a second model, CCSM4, which was examined for comparison purposes. The primary findings include the following:

- The ongoing and projected retreat of sea ice is greatest in autumn, which is the season of greatest expected impacts on extratropical cyclones.
- The models reproduce the observed seasonality of the sea ice loss and the general patterns of sea level pressure (SLP) and cyclone metrics, although the storm tracks (densities) and intensities are somewhat less sharp relative to ERA-I because of the models' coarser resolution. Such differences can be expected to decrease with potential higher resolution in newer model versions.
- The projected changes in storm intensity (as well as sea ice, SLP and precipitation) appear to scale generally linearly with the RCP value of the forcing scenario and with time through the 21st century.
- A significant projected decrease of the SLP over the Arctic Ocean during the 21st century is at least partly a consequence of the diminishing sea ice cover on the same time scales. Pressures are projected to increase farther south, significantly over the North Atlantic Ocean, consistent with a northward shift of the storm tracks.
- Projected patterns of changes in cyclone intensity over high-latitudes show general increases, especially over the Alaskan region, although there are some areas of projected decreases in intensity. The projected increases in intensity tend to migrate southwards from the Arctic Ocean to the subarctic latitudes through the autumn period.

GMDD
7, 8975–9015, 2014

- Projected changes in track density are much less coherent, although there is a general tendency towards less frequent storms in midlatitudes and more frequent storms in high-latitudes. Relatively large increases in frequency are projected for the Baffin Bay/Davis Strait region.

- Over the whole domain circumpolar north of 40° N, there is a tendency of slightly fewer and weaker cyclones towards the end of the century. However, the reduction in frequency (4 %) is larger than intensity (2 %), indicating that changes in cyclone strength do not correlate proportionally to cyclone frequency.

- Autumn precipitation is projected to increase significantly across the entire high-latitudes. Together with the projected increases in storm intensity and sea level and the loss of sea ice, this increase implies a greater vulnerability to coastal flooding and erosion, especially in the Alaskan region.

The results reported here are limited to two climate models and to two simulations by each model, one with a low emission scenario (RCP 4.5) and one with a high (business-as-usual) scenario (RCP 8.5). The projected changes appear to scale linearly with the intensity of the RCP forcing. The robustness of such results obtained would be enhanced by the inclusion of additional models and ensemble members. However, the results obtained from the two different models show enough similarities that the conclusions listed above can be taken as starting points in assessments of the likely changes in storm activity in the northern high-latitudes.

As additional models and ensemble members are included in assessments of future changes in Arctic cyclone activity, the relative importance of internal variability (deduced from different ensemble members of a single model) and model-derived uncertainty (deduced from across-model differences in cyclone statistics) will be important to an assessment of uncertainties. Should across-model differences dominate (as they do with temperature, for example), priority must be given to diagnosing the reasons why the models are different. It may also be fruitful to explore model selection ("filtering") strategies based on the fidelity of the models to the observed data on cyclone activity.

GMDD
7, 8975–9015, 2014

Both wind and precipitation changes are likely to have costly impacts on human society, especially on top of sea level rise. This adds to the importance of reducing the uncertainties in future changes of Arctic cyclone activity and related variables that will impact northern coasts, communities and offshore activities.

Author contributions. The authors shared the task of designing and evaluating the study, while E. M. Knudsen carried out the data acquisition and analysis. E. M. Knudsen also prepared the manuscript, but with significant contributions from J. E. Walsh.

Acknowledgements. We thank K. I. Hodges for providing the TRACK algorithm and guidance on *p* value calculations for the storm track parameters. We are grateful to A. Sorteberg for his helpful internal review of an earlier version of this manuscript. The data for this paper are available at Program for Climate Model Diagnosis and Intercomparison's web page CMIP5 Coupled Model Intercomparison Project (http://cmip-pcmdi.llnl.gov/cmip5/index.html) and at ECMWF's ERA-I web access (http://apps.ecmwf.int/datasets/data/interim_full_moda/). The work was financially supported by the Research Council of Norway through the BlueArc project (no. 207650) and by the U.S. National Science Foundation through Grants ARC-1023131 and ARC-1049225.

References

AMAP: Snow, water, ice and permafrost in the Arctic (SWIPA): Climate change and the cryosphere, Tech. rep., Arctic Monitoring and Assessment Programme (AMAP), Oslo, Norway, 2011. 8977

Barnes, E.: Revisiting the evidence linking Arctic amplification to extreme weather in midlatitudes, Geophys. Res. Lett., 40, 4734–4739, doi:10.1002/grl.50880, 2013. 8977

Barnes, E., Dunn-Sigouin, E., Masato, G., and Woollings, T.: Exploring recent trends in Northern Hemisphere blocking, Geophys. Res. Lett., 41, 638–644, doi:10.1002/2013GL058745, 2014. 8977

Bekryaev, R., Polyakov, I., and Alexeev, V.: Role of polar amplification in long-term surface air temperature variations and modern Arctic warming, J. Climate, 23, 3888–3906, doi:10.1175/2010JCLI3297.1, 2010. 8977

GMDD
7, 8975–9015, 2014

Bengtsson, L., Hodges, K., and Roeckner, E.: Storm tracks and climate change, J. Climate, 19, 3518–3543, doi:10.1175/JCLI3815.1, 2006. 8993

Bengtsson, L., Hodges, K., and Keenlyside, N.: Will extratropical storms intensify in a warmer climate?, J. Climate, 22, 2276–2301, doi:10.1175/2008JCLI2678.1, 2009. 8993, 8994

Bentsen, M., Bethke, I., Debernard, J. B., Iversen, T., Kirkevåg, A., Seland, Ø., Drange, H., Roelandt, C., Seierstad, I. A., Hoose, C., and Kristjánsson, J. E.: The Norwegian Earth System Model, NorESM1-M – Part 1: Description and basic evaluation of the physical climate, Geosci. Model Dev., 6, 687–720, doi:10.5194/gmd-6-687-2013, 2013. 8979

Bleck, R., Rooth, C., Hu, D., and Smith, L.: Salinity-driven thermocline transients in a wind-and thermohaline-forced isopycnic coordinate model of the North Atlantic, J. Phys. Oceanogr., 22, 1486–1505, doi:10.1175/1520-0485(1992)022<1486:SDTTIA>2.0.CO;2, 1992. 8979

Bracegirdle, T. and Gray, S.: An objective climatology of the dynamical forcing of polar lows in the Nordic seas, Int. J. Climatol., 28, 1903–1919, doi:10.1002/joc.1686, 2008. 8983

Chung, C. E., Cha, H., Vihma, T., Räisänen, P., and Decremer, D.: On the possibilities to use atmospheric reanalyses to evaluate the warming structure in the Arctic, Atmos. Chem. Phys., 13, 11209–11219, doi:10.5194/acp-13-11209-2013, 2013. 8980

Cohen, J., Furtado, J., Barlow, M., Alexeev, V., and Cherry, J.: Arctic warming, increasing snow cover and widespread boreal winter cooling, Environ. Res. Lett., 7, 014007, doi:10.1088/1748-9326/7/1/014007, 2012. 8977

Condron, A. and Renfrew, I.: The impact of polar mesoscale storms on northeast Atlantic Ocean circulation, Nat. Geosci., 6, 34–37, doi:10.1038/ngeo1661, 2013. 8982

Condron, A., Bigg, G., and Renfrew, I.: Polar mesoscale cyclones in the northeast Atlantic: comparing climatologies from ERA-40 and satellite imagery, Mon. Weather Rev., 134, 1518–1533, doi:10.1175/MWR3136.1, 2006. 8982

de Boer, G., Chapman, W., Kay, J., Medeiros, B., Shupe, M., Vavrus, S., and Walsh, J.: A characterization of the present-day Arctic atmosphere in CCSM4, J. Climate, 25, 2676–2695, doi:10.1175/JCLI-D-11-00228.1, 2012. 8980, 8984

Dee, D., Uppala, S., Simmons, A., Berrisford, P., Poli, P., Kobayashi, S., Andrae, U., Balmaseda, M., Balsamo, G., Bauer, P., Bechtold, P., Beljaars, A., van de Berg, L., Bidlot, J., Bormann, N., Delsol, C., Dragani, R., Fuentes, M., Geer, A., Haimberger, L., Healy, S., Hersbach, H., Hólm, E., Isaksen, L., Kållberg, P., Köhler, M., Matricardi, M., McNally, A., Monge-Sanz, B., Morcrette, J.-J., Park, B.-K., Peubey, C., de Rosnay, P., Tavolato, C., Thépaut, J.-N.,

GMDD
7, 8975–9015, 2014

and Vitart, F.: The ERA-Interim reanalysis: configuration and performance of the data assimilation system, Q. J. Roy. Meteor. Soc., 137, 553–597, doi:10.1002/qj.828, 2011. 8980
DeWeaver, E. and Bitz, C.: Atmospheric circulation and its effect on Arctic sea ice in CCSM3 simulations at medium and high resolution, J. Climate, 19, 2415–2436, doi:10.1175/JCLI3753.1, 2006. 8984
Drange, H., Gerdes, R., Gao, Y., Karcher, M., Kauker, F., and Bentsen, M.: Ocean general circulation modelling of the Nordic Seas, in: The Nordic Seas: an Integrated Perspective, edited by: Drange, H., Dokken, T., Furevik, T., Gerdes, R., and Berger, W., vol. 158, Wiley Online Library, Washington DC, USA, 199–219, 2005. 8979
Francis, J. and Vavrus, S.: Evidence linking Arctic amplification to extreme weather in mid-latitudes, Geophys. Res. Lett., 39, L06801, doi:10.1029/2012GL051000, 2012. 8977
Furevik, T., Bentsen, M., Drange, H., Kindem, I., Kvamstø, N., and Sorteberg, A.: Description and evaluation of the Bergen climate model: ARPEGE coupled with MICOM, Clim. Dynam., 21, 27–51, doi:10.1007/s00382-003-0317-5, 2003. 8979
Gent, P., Danabasoglu, G., Donner, L., Holland, M., Hunke, E., Jayne, S., Lawrence, D., Neale, R., Rasch, P., Vertenstein, M., Worley, P., Yang, Z.-L., and Zhang, M.: The Community Climate System Model version 4, J. Climate, 24, 4973–4991, doi:10.1175/2011JCLI4083.1, 2011. 8979
Held, I. and Soden, B.: Robust responses of the hydrological cycle to global warming, J. Climate, 19, 5686–5699, doi:10.1175/JCLI3990.1, 2006. 8994, 8995
Hodges, K.: A general method for tracking analysis and its application to meteorological data, Mon. Weather Rev., 122, 2573–2586, doi:10.1175/1520-0493(1994)122<2573:AGMFTA>2.0.CO;2, 1994. 8981
Hodges, K.: Feature tracking on the unit-sphere, Mon. Weather Rev., 123, 3458–3465, doi:10.1175/1520-0493(1995)123<3458:FTOTUS>2.0.CO;2, 1995. 8981
Hodges, K.: Spherical nonparametric estimators applied to the UGAMP model integration for AMIP, Mon. Weather Rev., 124, 2914–2932, doi:10.1175/1520-0493(1996)124<2914:SNEATT>2.0.CO;2, 1996. 8982
Hodges, K.: Adaptive constraints for feature tracking, Mon. Weather Rev., 127, 1362–1373, doi:10.1175/1520-0493(1999)127<1362:ACFFT>2.0.CO;2, 1999. 8981
Hodges, K.: Confidence intervals and significance tests for spherical data derived from feature tracking, Mon. Weather Rev., 136, 1758–1777, doi:10.1175/2007MWR2299.1, 2008. 8982

GMDD
7, 8975–9015, 2014

Hodges, K., Hoskins, B., Boyle, J., and Thorncroft, C.: A comparison of recent reanalysis datasets using objective feature tracking: Storm tracks and tropical easterly waves, Mon. Weather Rev., 131, 2012–2037, doi:10.1175/1520-0493(2003)131<2012:ACORRD>2.0.CO;2, 2003. 8981

Hodges, K., Lee, R., and Bengtsson, L.: A comparison of extratropical cyclones in recent reanalyses ERA-Interim, NASA MERRA, NCEP CFSR, and JRA-25, J. Climate, 24, 4888–4906, doi:10.1175/2011JCLI4097.1, 2011. 8980, 8985

Iversen, T., Bentsen, M., Bethke, I., Debernard, J. B., Kirkevåg, A., Seland, Ø., Drange, H., Kristjansson, J. E., Medhaug, I., Sand, M., and Seierstad, I. A.: The Norwegian Earth System Model, NorESM1-M – Part 2: Climate response and scenario projections, Geosci. Model Dev., 6, 389–415, doi:10.5194/gmd-6-389-2013, 2013. 8979

Jakobson, E., Vihma, T., Palo, T., Jakobson, L., Keernik, H., and Jaagus, J.: Validation of atmospheric reanalyses over the central Arctic Ocean, Geophys. Res. Lett., 39, L10802, doi:10.1029/2012GL051591, 2012. 8980

Kang, S. and Lu, J.: Expansion of the Hadley cell under global warming: winter versus summer, J. Climate, 25, 8387–8393, doi:10.1175/JCLI-D-12-00323.1, 2012. 8994

Karl, T., Melillo, J., and Peterson, T. (Eds.): Global climate change impacts in the United States, Tech. rep., U.S. Global Change Research Program (USGRP), Cambridge, UK and New York, USA, 2009. 8978

Kirkevåg, A., Iversen, T., Seland, Ø., Hoose, C., Kristjánsson, J. E., Struthers, H., Ekman, A. M. L., Ghan, S., Griesfeller, J., Nilsson, E. D., and Schulz, M.: Aerosol–climate interactions in the Norwegian Earth System Model – NorESM1-M, Geosci. Model Dev., 6, 207–244, doi:10.5194/gmd-6-207-2013, 2013. 8979

Langehaug, H., Geyer, F., Smedsrud, L., and Gao, Y.: Arctic sea ice decline and ice export in the CMIP5 historical simulations, Ocean Model., 71, 114–126, doi:10.1016/j.ocemod.2012.12.006, 2013. 8981

Maier-Reimer, E.: Geochemical cycles in an ocean general circulation model. Preindustrial tracer distributions, Global Biogeochem. Cy., 7, 645–677, doi:10.1029/93GB01355, 1993. 8980

Maier-Reimer, E., Kriest, I., Segschneider, J., and Wetzel, P.: The HAMburg Ocean Carbon Cycle Model HAMOCC 5.1 – Technical description release 1.1, Tech. rep., Max Planck Institute for Meteorology, Hamburg, Germany, 2005. 8980

GMDD
7, 8975–9015, 2014

McCabe, G., Clark, M., and Serreze, M.: Trends in Northern Hemisphere surface cyclone frequency and intensity, J. Climate, 14, 2763–2768, doi:10.1175/1520-0442(2001)014<2763:TINHSC>2.0.CO;2, 2001. 8978, 8989, 8991

Melillo, J., Richmond, T., and Yohe, G. (Eds.): Climate change impacts in the United States, Tech. rep., U.S. Global Change Research Program (USGRP), Washington DC, USA, 2014. 8978

Mesquita, M., Atkinson, D., and Hodges, K.: Characteristics and variability of storm tracks in the North Pacific, Bering Sea, and Alaska*, J. Climate, 23, 294–311, doi:10.1175/2009JCLI3019.1, 2010. 8978

Neu, U., Akperov, M., Bellenbaum, N., Benestad, R., Blender, R., Caballero, R., Cocozza, A., Dacre, H., Feng, Y., Fraedrich, K., Grieger, J., Gulev, S., Hanley, J., Hewson, T., Inatsu, M., Keay, K., Kew, S., Kindem, I., Leckebusch, G., Liberato, M., Lionello, P., Mokhov, I., Pinto, J., Raible, C., Reale, M., Rudeva, I., Schuster, M., Simmonds, I., Sinclair, M., Sprenger, M., Tilinina, N., Trigo, I., Ulbrich, S., Ulbrich, U., Wang, X., and Wernli, H.: IMILAST: a community effort to intercompare extratropical cyclone detection and tracking algorithms, B. Am. Meteorol. Soc., 94, 529–547, doi:10.1175/BAMS-D-11-00154.1, 2013. 8981

Orsolini, Y. and Sorteberg, A.: Projected changes in Eurasian and Arctic summer cyclones under global warming in the Bergen Climate Model, Atmos. Ocean. Sci. Lett., 2, 62–67, 2009. 8991

Overland, J. and Wang, M.: Large-scale atmospheric circulation changes are associated with the recent loss of Arctic sea ice, Tellus A, 62, 1–9, doi:10.1111/j.1600-0870.2009.00421.x, 2010. 8977

Overland, J., Wang, M., Walsh, J., and Stroeve, J.: Future Arctic climate changes: adaptation and mitigation time scales, Earth's Future, 2, 68–74, doi:10.1002/2013EF000162, 2013. 8988

Pithan, F. and Mauritsen, T.: Arctic amplification dominated by temperature feedbacks in contemporary climate models, Nat. Geosci., 7, 181–184, doi:10.1038/ngeo2071, 2014. 8977

Rogers, T. S., Walsh, J. E., Rupp, T. S., Brigham, L. W., and Sfraga, M.: Future Arctic marine access: analysis and evaluation of observations, models, and projections of sea ice, The Cryosphere, 7, 321–332, doi:10.5194/tc-7-321-2013, 2013. 8981

Screen, J. and Simmonds, I.: Exploring links between Arctic amplification and mid-latitude weather, Geophys. Res. Lett., 40, 959–964, doi:10.1002/GRL.50174, 2013. 8977

GMDD
7, 8975–9015, 2014

Sepp, M. and Jaagus, J.: Changes in the activity and tracks of Arctic cyclones, Climatic Change, 105, 577–595, doi:10.1007/s10584-010-9893-7, 2011. 8989, 8991, 8992

Sorteberg, A. and Walsh, J.: Seasonal cyclone variability at 70° N and its impact on moisture transport into the Arctic, Tellus A, 60, 570–586, doi:10.1111/j.1600-0870.2008.00314.x, 2008. 8985, 8989

Stocker, T., Qin, D., Plattner, G.-K., Tignor, M., Allen, S., Boschung, J., Nauels, A., Xia, Y. V. B., and Midgley, P. (Eds.): Climate change 2013: The physical science basis. Contribution of Working Group I to the Fifth Assessment Report of the Intergovernmental Panel on Climate Change, Tech. rep., Intergovernmental Panel on Climate Change (IPCC), Cambridge, United Kingdom and New York, USA, 2013. 8977, 8992, 8994, 8995

Stroeve, J., Kattsov, V., Barrett, A., Serreze, M., Pavlova, T., Holland, M., and Meier, W.: Trends in Arctic sea ice extent from CMIP5, CMIP3 and observations, Geophys. Res. Lett., 39, L16502, doi:10.1029/2012GL052676, 2012. 8981

Thompson, D. and Wallace, J.: Regional climate impacts of the Northern Hemisphere annular mode, Science, 293, 85–89, doi:10.1126/science.1058958, 2001. 8989

Tilinina, N., Gulev, S., and Bromwich, D.: New view of Arctic cyclone activity from the Arctic system reanalysis, Geophys. Res. Lett., 41, 1766–1772, doi:10.1002/2013GL058924, 2014. 8985

Tjiputra, J. F., Assmann, K., Bentsen, M., Bethke, I., Otterå, O. H., Sturm, C., and Heinze, C.: Bergen Earth system model (BCM-C): model description and regional climate-carbon cycle feedbacks assessment, Geosci. Model Dev., 3, 123–141, doi:10.5194/gmd-3-123-2010, 2010. 8980

van Vuuren, D., Edmonds, J., Kainuma, M., Riahi, K., Thomson, A., Hibbard, K., Hurtt, G., Kram, T., Krey, V., Lamarque, J.-F., Masui, T., Meinshausen, M., Nakicenovic, N., Smith, S., and Rose, S.: The representative concentration pathways: an overview, Climatic Change, 109, 5–31, doi:10.1007/s10584-011-0148-z, 2011. 8981

Vose, R., Applequist, S., Bourassa, M., Pryor, S., Barthelmie, R., Blanton, B., Bromirski, P., Brooks, H., DeGaetano, A., Dole, R., Easterling, D., Jensen, R., Karl, T., Katz, R., Klink, K., Kruk, M., Kunkel, K., MacCracken, M., Peterson, T., Shein, K., Thomas, B., Walsh, J., Wang, X., Wehner, M., Wuebbles, D., and Young, R.: Monitoring and understanding changes in extremes: extratropical storms, winds, and waves, B. Am. Meteorol. Soc., 95, 377–386, doi:10.1175/BAMS-D-12-00162.1, 2014. 8993

GMDD
7, 8975–9015, 2014

Walsh, J., Chapman, W., Romanovsky, V., Christensen, J., and Stendel, M.: Global climate model performance over Alaska and Greenland, J. Climate, 21, 6156–6174, doi:10.1175/2008JCLI2163.1, 2008. 8980

Wang, X., Swail, V., and Zwiers, F.: Climatology and changes of extratropical cyclone activity: comparison of ERA-40 with NCEP-NCAR reanalysis for 1958–2001, J. Climate, 19, 3145–3166, doi:10.1175/JCLI3781.1, 2006. 8978, 8989

Wang, X., Feng, Y., Compo, G., Swail, V., Zwiers, F., Allan, R., and Sardeshmukh, P.: Trends and low frequency variability of extra-tropical cyclone activity in the ensemble of twentieth century reanalysis, Clim. Dynam., 40, 2775–2800, doi:10.1007/s00382-012-1450-9, 2013. 8978, 8989, 8991

Zahn, M. and von Storch, H.: A long-term climatology of North Atlantic polar lows, Geophys. Res. Lett., 35, L22702, doi:10.1029/2008GL035769, 2008. 8983

Zappa, G., Shaffrey, L., and Hodges, K.: The ability of CMIP5 models to simulate North Atlantic extratropical cyclones, J. Climate, 26, 5379–5396, doi:10.1175/JCLI-D-12-00501.1, 2013. 8980, 8985, 8986

Zhang, X., Walsh, J., Zhang, J., Bhatt, U., and Ikeda, M.: Climatology and interannual variability of Arctic cyclone activity: 1948–2002, J. Climate, 17, 2300–2317, doi:10.1175/1520-0442(2004)017<2300:CAIVOA>2.0.CO;2, 2004. 8978

GMDD
7, 8975–9015, 2014

Table 1. Decadal mean Arctic sea ice extent monthly averages for 2000's, 2050's and 2090's and changes for the two latter decades compared to the former, following the RCP8.5 scenario. First number within each row from NorESM; second number within each row from CCSM. Unit 10^6 km^2.

Decade	Jan	Feb	Mar	Apr	May	Jun	Jul	Aug	Sep	Oct	Nov	Dec
2000's	13.1	14.0	14.7	14.2	13.3	11.7	10.2	9.0	7.8	9.2	10.6	12.1
	12.4	13.0	13.2	12.8	11.9	10.4	8.7	6.6	5.5	7.3	8.8	10.8
2050's	10.7	11.9	12.7	12.5	11.5	9.9	8.3	6.9	5.5	6.0	7.1	8.9
	10.0	10.8	11.2	10.8	10.3	9.1	5.3	0.8	0.8	1.1	4.4	7.8
2090's	8.8	10.1	11.1	11.0	9.7	7.6	4.8	2.3	0.3	1.4	3.7	6.2
	6.6	9.1	9.9	9.8	9.3	7.2	1.7	0	0	0	0.3	2.8
Δ2050's	−2.4	−2.1	−2.0	−1.7	−1.8	−1.8	−1.9	−2.1	−2.3	−3.2	−3.5	−3.2
	−2.4	−2.2	−2.0	−2.0	−1.6	−1.3	−3.4	−5.8	−4.7	−6.2	−4.4	−3.0
Δ2090's	−4.3	−3.9	−3.6	−3.2	−3.6	−4.1	−5.4	−6.7	−7.5	−7.8	−6.9	−5.9
	−5.8	−3.9	−3.3	−3.0	−2.6	−3.2	−7.0	−6.6	−5.5	−7.3	−8.5	−8.0

GMDD
7, 8975–9015, 2014

Table 2. Time period mean sea level pressure (SLP), track density (tden), mean intensity (mint) and precipitation (P) SOND averages and changes for 1979–2005 and 2074–2100 relative to 1979–2005 for the RCP8.5 scenario (Δ2074–2100) in ERA-I, NorESM and CCSM. First number within each column denotes average over midlatitudes (40–65° N); second number within each column denotes average over high-latitudes (65–90° N). For 1979–2005, units are hPa, no. dens $(\text{month})^{-1}$ $(10^6\ \text{km}^2)^{-1}$, $10^{-5}\ \text{s}^{-1}$ and mmd^{-1} for SLP, tden, mint and Ptot, respectively. For Δ2074–2100, unit is %.

Data set	Time period	SLP		tden		mint		P	
ERA-I	1979–2005	1015	1012	9.0	7.0	4.2	3.7	2.5	1.2
NorESM	1979–2005	1016	1010	8.9	6.8	4.0	3.8	2.5	1.2
	Δ2074–2100	0.02	−0.24	−3.9	0.3	−0.2	0.9	10.7	38.2
CCSM	1979–2005	1015	1006	9.5	7.7	4.2	3.9	2.8	1.4
	Δ2074–2100	0.02	−0.18	−6.5	−0.8	−1.7	2.9	8.0	31.8

GMDD
7, 8975–9015, 2014

Table 3. Changes of track density (tden; first row), mean intensity (mint; second row) and precipitation (*P*; third row) over Sep and Dec for 2074–2100 relative to 1979–2005 for the RCP8.5 scenario in NorESM and CCSM in four North Atlantic and North Pacific storm track regions. The regions are western North America (WNA; 50–58° N, 125–137° W and 58–62° N, 136–155° W), Bering and western Alaska (BWA; 55–72° N, 155–180° W), northwestern Europe (NWE; 55–65° N, 15° W–15° E) and northeastern Europe (NEE; 65–75° N, 10° W–50° E). First number within each column denotes change in Sep; second number within each column denotes change in Dec. Unit %.

Parameter	Data set	WNA		BWA		NWE		NEE	
tden	NorESM	−20.1	18.2	11.3	−13.4	12.8	10.2	−6.5	−0.8
	CCSM	−8.0	−12.8	−8.1	15.5	−21.7	1.2	−1.2	−11.6
mint	NorESM	−6.2	0	−1.4	3.2	−5.9	4.2	−0.1	1.5
	CCSM	−5.2	−0.5	2.0	8.3	−8.9	1.3	0.9	−3.6
P	NorESM	−4.1	15.5	23.8	21.5	5.7	19.7	11.7	21.1
	CCSM	5.8	10.1	18.0	44.4	−12.0	8.7	13.0	5.3

GMDD
7, 8975–9015, 2014

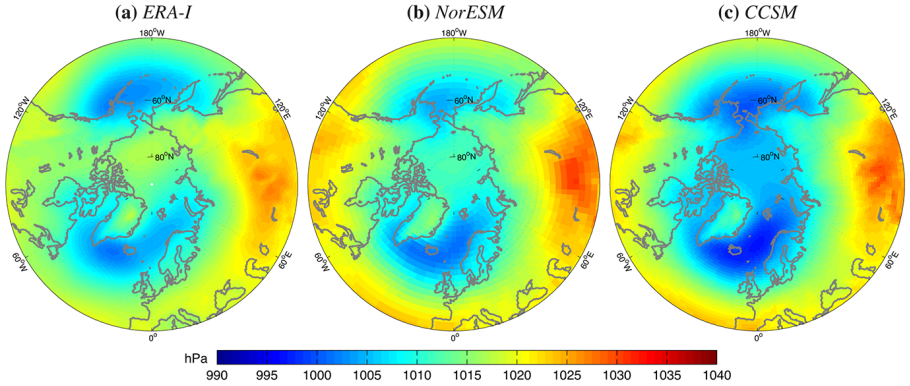

Figure 1. Average sea level pressures for SOND 1979–2005 in **(a)** ERA-I, **(b)** NorESM and **(c)** CCSM.

GMDD
7, 8975–9015, 2014

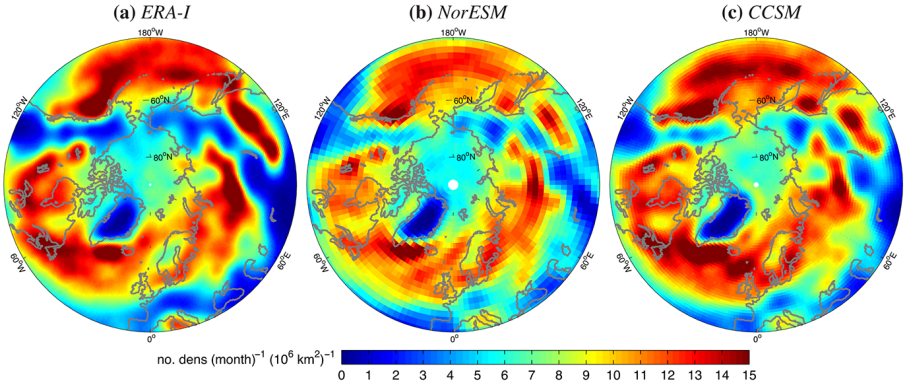

Figure 2. Average track densities for SOND 1979–2005 in **(a)** ERA-I, **(b)** NorESM and **(c)** CCSM.

GMDD
7, 8975–9015, 2014

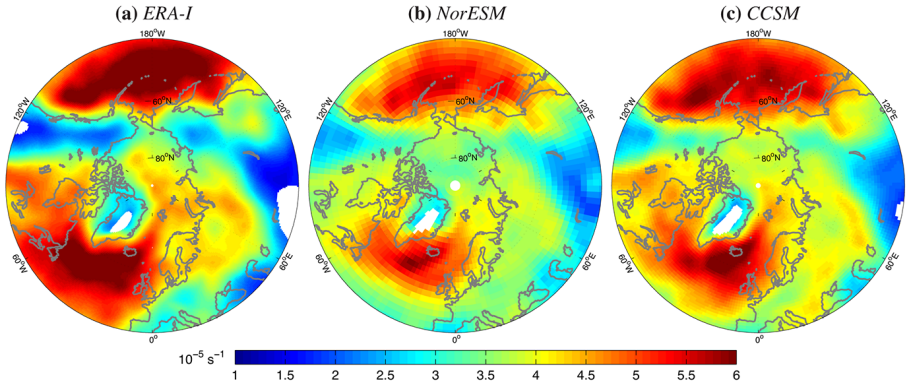

Figure 3. Average mean intensities for SOND 1979–2005 in **(a)** ERA-I, **(b)** NorESM and **(c)** CCSM. Regions with track density below 0.5 no. density (month)$^{-1}$ (10^6 km^2)$^{-1}$ are shaded white.

GMDD
7, 8975–9015, 2014

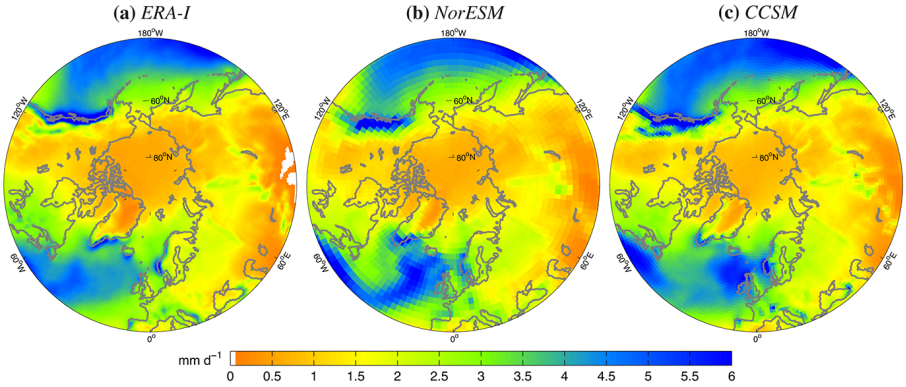

Figure 4. Average precipitations for SOND 1979–2005 in **(a)** ERA-I, **(b)** NorESM and **(c)** CCSM.

GMDD
7, 8975–9015, 2014

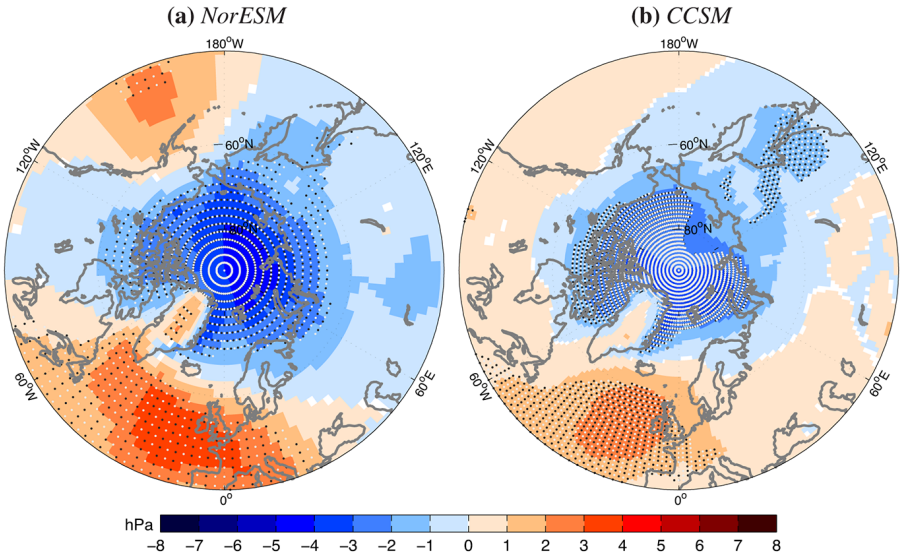

Figure 5. Average sea level pressures for SOND 2074–2100 relative to 1979–2005 for the RCP8.5 scenario in **(a)** NorESM and **(b)** CCSM. Alternating black and white dots mark regions of significant change at a 95 % confidence level.

GMDD
7, 8975–9015, 2014

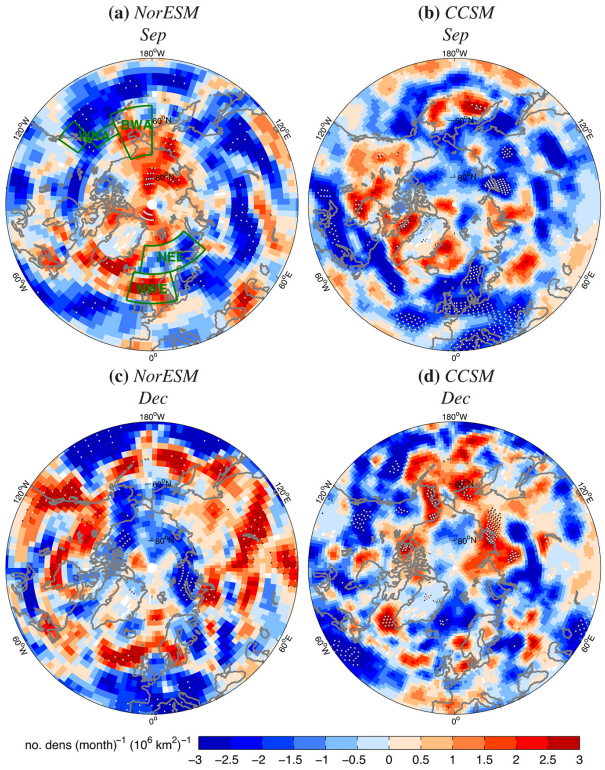

Figure 6. Average track densities for September (upper row) and December (lower row) 2074–2100 relative to 1979–2005 for the RCP8.5 scenario in **(a)**, **(c)** NorESM and **(b)**, **(d)** CCSM. Alternating black and white dots mark regions where $p < 0.05$ based on 2000 samples. Green boxes in **(a)** show the four regions in Table 3.

GMDD
7, 8975–9015, 2014

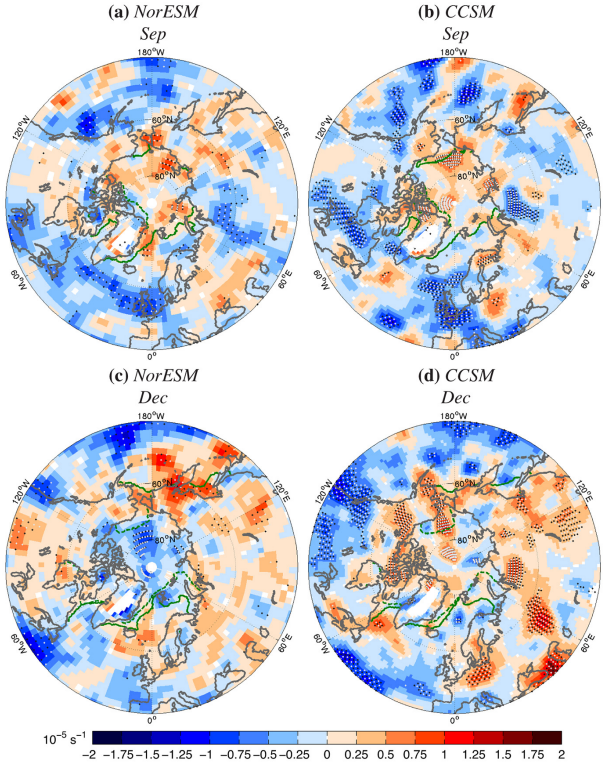

Figure 7. Average mean intensities for September (upper row) and December (lower row) 2074–2100 relative to 1979–2005 for the RCP8.5 scenario in **(a)**, **(c)** NorESM and **(b)**, **(d)** CCSM. Regions with track density below 0.5 no. density $(\text{month})^{-1}\,(10^6\,\text{km}^2)^{-1}$ in the historical time period are shaded white. Alternating black and white dots mark regions where $p < 0.05$ based on 2000 samples. Solid and dashed green lines show the sea ice boundaries in each model and month over 1979–2005 and RCP8.5 2074–2100, respectively, calculated using a threshold of 15 % SIC.

GMDD
7, 8975–9015, 2014

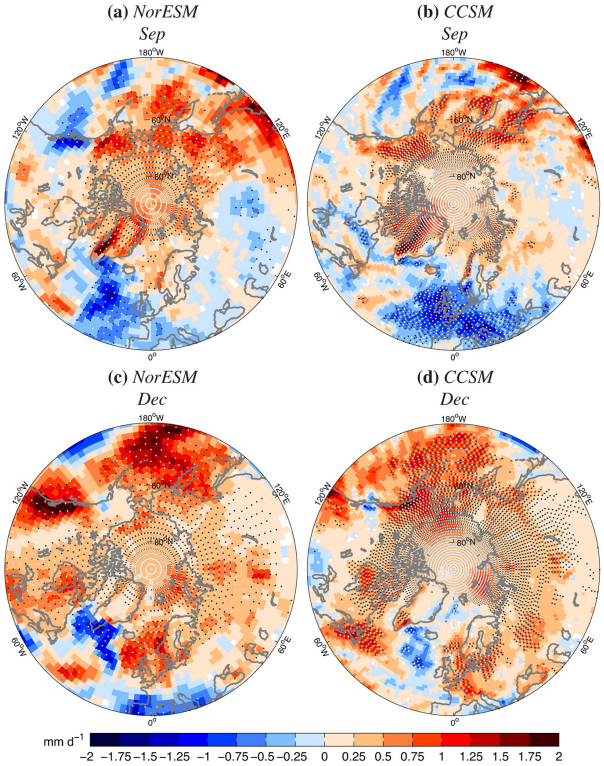

Figure 8. Average precipitations for September (upper row) and December (lower row) 2074–2100 relative to 1979–2005 for the RCP8.5 scenario in **(a)**, **(c)** NorESM and **(b)**, **(d)** CCSM. Alternating black and white dots mark regions of significant change at a 95 % confidence level.

GMDD
7, 8975–9015, 2014